2024 European Control Conference (ECC)
June 25-28, 2024. Stockholm, Sweden

Transient Solutions of the Fokker-Planck Equation using a Galerkin-Method with Weighted Test Functions

Wolfram Martens[1] and Riccardo Ferrari[1]

Abstract— **This article addresses the computation of stationary and transient solutions of the Fokker-Planck equation for nonlinear stochastic processes. We extend a Galerkin-method, which was previously used to compute stationary solutions for nonlinear mechanical systems, by a generalized formulation of the test function space, including the original approach as a limit. The use of weighted test functions improves the performance in the stationary setting and enables the computation of transient solutions. The properties of the resulting linear system of equations are discussed, and results for stationary and transient probability density functions for nonlinear 1D-, 2D- and 4D-systems are presented.**

I. INTRODUCTION

The ability to assess the probabilistic behaviour of dynamical systems under uncertainty is essential for the safe operation of modern technical systems. Example applications of uncertainty propagation include, but are not limited to, stochastic optimal control [1], [2], model predictive control [3], [4], probabilistic model validation [5] and nonlinear filtering [6]–[8].

Many stochastic dynamical systems can be modeled by diffusion processes (DPs), for which the probability density function (pdf) can be computed via the Fokker-Planck equation (FPE), a partial differential equation in the pdf [9]. The example of nonlinear filtering illustrates how solutions of the FPE have the potential to fill a gap among the most commonly used techniques for nonlinear stochastic systems. One important class of filters builds on parametric representations of the pdf, most prominently using its first- and second-order moments, as in nonlinear extensions of the Kalman-Filter (KF). Advanced filters also track higher-order moments, but linearization errors and over-simplification can result in filter inconsistency and divergence [7]. Sequential Monte-Carlo methods represent a non-parametric alternative for complex pdfs and highly nonlinear systems [8]. Particle filters (PFs) are broadly applicable, even for high-dimensional systems, and are the de-facto standard where KF extensions are insufficient. However, the point-wise pdf representation gives rise to sample empoverishment and degeneracy for many PF implementations [10].

Solving the FPE in practice is still a fundamental challenge, and various numerical computation methods exist in the literature. In [11] a simple Finite-Difference method (FDM) is used to propagate the pdf between measurements, whereas [12] demonstrates the use of a meshless partition-of-unity Finite-Element method (FEM). [13] uses proximal recursion to transform the problem to a smooth convex optimization, avoiding discretization of the state space. Other numerical FPE solution methods include cell-to-cell mapping [14] and the path-integral method [15].

This article builds on a Galerkin-method that expands initial pdf approximations in a finite-dimensional function space [16], [17]. Extensions and technical applications of this approach were discussed in [18], [19], but only for stationary FPE solutions. Unlike FEM, another instance of the Galerkin-method, our approach avoids state space discretization and supports infinite supports, rather than assuming a finite domain outside of which the pdf is zero. Furthermore, it is possible, but not necessary, to include prior knowledge about the exact pdf.

The main contributions are the following. We propose a generalization of the test function space by means of additional weighting functions, including [18] as a limit. The structure and characteristic properties of the resulting linear system are discussed for a specific class of basis functions. We propose a hyperbolic index truncation (HIT) scheme, as previously applied in Polynomial Chaos expansion [20]–[22], to manage the computational cost for higher-dimensional systems. Results are presented for stationary and transient FPE solutions, with an improved performance over [18].

The paper is structured as follows. Section II discusses the Galerkin-method and the generalized formulation of the test function space for 1D-systems. Section III examines the resulting linear system, which is extended in Section IV to the multivariate case. Section V presents results for 1D-, 2D- and 4D-systems, using exact solutions and Monte-Carlo simulation (MCS) as reference. Finally, Section VI provides a summary of our contributions and a discussion.

II. GENERAL CONCEPT

A 1D-DP is used to outline the general concept of the approach in [18] and our proposed extensions.

Notation: We use non-bold letters for scalar expressions, and bold-face letters for vectors (lower-case) and matrices (upper-case). Random variables are denoted by upper-case upright letters.

A. Diffusion process and FPE

Definition 1 (1D-diffusion process): The stochastic differential equation in Itô-form

$$\mathrm{d}\mathrm{X}_t = f(t, \mathrm{X}_t)\mathrm{d}t + g(t, \mathrm{X}_t)\mathrm{d}\mathrm{W}_t, \tag{1}$$

describes a 1D-diffusion process X_t, where dW_t denotes the increment of a 1D-Wiener process.

[1]Both authors are with Delft Center for Systems and Control, TUDelft, Netherlands {w.martens,r.ferrari}@tudelft.nl

Definition 2 (1D-Fokker-Planck equation): The joint pdf $p(t,x)$ of X_t is described by the 1D-FPE [9]

$$\dot{p}(t,x) = -\left(f(t,x)p(t,x)\right)' + \frac{1}{2}\left(b(t,x)p(t,x)\right)'', \quad (2)$$

where $b(t,x) = g(t,x)^2$, and $\dot{()}$ and $()', ()''$ denote partial derivatives with respect to t and x, respectively.

Assumption 1 (Polynomial drift and diffusion): Throughout the paper, we assume time-invariant, polynomial drift and diffusion terms, $f(t,x) = f(x) = \sum_{i=0}^{N_f} a_i^f x^i$ and $b(t,x) = b(x) = \sum_{i=0}^{N_b} a_i^b x^i$.

B. Approximate solution and weak FPE formulation

Exact solutions $p(t,x)$ of (2) are known only for very limited classes of problems (some of which will be used as reference solutions in this paper). Hence, for realistic applications one should resort to numerical FPE solutions.

Our approach considers approximations $\tilde{p}(t,x)$ of the form

$$\tilde{p}(t,x) = \sum_{n=0}^{N} c_n(t)u_n(x) = \boldsymbol{u}(x)^T\boldsymbol{c}(t), \quad (3)$$

where $\boldsymbol{u}(x) = [u_0(x), \cdots, u_N(x)]^T$ is a basis of an $(N+1)$-dimensional function space U in the state variable x. For constant $c_n(t) = c_n$, (3) reduces to the approach in [18].

Definition 3 (FPE Residual): The FPE residual for the approximate solution reads $R(\tilde{p}) = -\dot{\tilde{p}} - \left(f\tilde{p}\right)' + \frac{1}{2}\left(b\tilde{p}\right)''$.

The expansion coefficients $\boldsymbol{c}(t)$ are determined in the sense of a Galerkin-method, where $R(\tilde{p})$ is required to be orthogonal to an $(N+1)$-dimensional test function space V. Assuming that $\boldsymbol{v}(x) = [v_0(x), \cdots, v_N(x)]^T$ is a basis of V, we can write

$$\langle \boldsymbol{v}, R(\tilde{p})\rangle_{L_2} = \int_{\mathbb{R}} \boldsymbol{v}(x)R(\tilde{p}(x))\mathrm{d}x = \boldsymbol{0}. \quad (4)$$

If we further select $\boldsymbol{u}(x), \boldsymbol{v}(x)$, such that $\langle v_m, u_n\rangle = \delta_{mn}$, where δ_{mn} denotes the Kronecker symbol, we get

$$\dot{\boldsymbol{c}}(t) = \underbrace{\left(\boldsymbol{H}^f + \frac{1}{2}\boldsymbol{H}^b\right)}_{\boldsymbol{H}}\boldsymbol{c}(t), \text{ where} \quad (5)$$

$$\boldsymbol{H}^f = -\int_{\mathbb{R}} \boldsymbol{v}(x)\left(f(x)\boldsymbol{u}(x)^T\right)'\mathrm{d}x, \quad (6)$$

$$\boldsymbol{H}^b = \int_{\mathbb{R}} \boldsymbol{v}(x)\left(b(x)\boldsymbol{u}(x)^T\right)''\mathrm{d}x. \quad (7)$$

C. Eigenvalues of $\boldsymbol{H}$ for ergodic system

If a unique stationary pdf $p_{\text{stat}}(x)$ exists for the FPE with $\dot{p} = 0$ in (2), then we expect a non-trivial and unique constant solution for $\boldsymbol{c}(t) = \boldsymbol{c}_{\text{stat}}$, which solves

$$\boldsymbol{0} = \boldsymbol{H}\boldsymbol{c}_{\text{stat}}. \quad (8)$$

Hence, $\boldsymbol{H}$ should have a rank-defect of exactly 1, corresponding to a single 0-eigenvalue. Furthermore, if the diffusion process is ergodic, such that $p(t,x) \to p_{\text{stat}}(x)$ for $t \to \infty$, we expect that $\boldsymbol{c}(t) \to \boldsymbol{c}_{\text{stat}}$ in (5), and hence that all non-zero eigenvalues of $\boldsymbol{H}$ are negative.

D. Solution and test function space

As in [18], the solution functions $u_n(x)$ are defined as products of polynomials $a_n(x) = \sum_{i=0}^{n}\alpha_{ni}x^i$ with an initial approximation of the (time-invariant) pdf $p_0(x)$. Let $\boldsymbol{a}(x) = [a_0(x), \cdots, a_N(x)]^T$ denote a polynomial basis up to order N, so that $\boldsymbol{u}(x) = \boldsymbol{a}(x)p_0(x)$ represents a basis of U. The approximate solution $\tilde{p}(t,x)$ then reads

$$\tilde{p}(t,x) = \boldsymbol{u}(x)^T\boldsymbol{c}(t) = \boldsymbol{a}(x)^T p_0(x)\boldsymbol{c}(t). \quad (9)$$

Contrary to [18], we select the test function space as products of polynomials with an additional weighting function $p_w(x)$,

$$\boldsymbol{v}(x) = \zeta\boldsymbol{a}(x)p_w(x) \quad (10)$$

with normalizing constant ζ. $p_w(x)$ and $p_0(x)$ are generally different, but both are valid pdfs with $p(x) \geq 0, \forall x \in \mathbb{R}$ and $\int_{\mathbb{R}} p(x)\ \mathrm{d}x = 1$.

Assumption 2: Being regular pdfs, we assume that $p_0(x)$ and $p_w(x)$ and their derivatives vanish for $|x| \to \infty$.

As a result, integration by parts of (6) and (7) yields

$$\boldsymbol{H}^f = \int_{\mathbb{R}} \boldsymbol{v}'(x)f(x)\boldsymbol{u}(x)^T\mathrm{d}x \quad (11)$$

$$\boldsymbol{H}^b = \int_{\mathbb{R}} \boldsymbol{v}''(x)b(x)\boldsymbol{u}(x)^T\mathrm{d}x. \quad (12)$$

We introduce the *combined pdf* $p_c(x) = \zeta p_0(x)p_w(x)$, where ζ is the same as in (10) and is chosen such that $\int_{\mathbb{R}} p_c(x)\ \mathrm{d}x = 1$. The polynomials $a_n(x)$ are defined to be orthogonal with $p_c(x)$ as weighting function,

$$\langle a_m, a_n\rangle_{p_c} = \int_{\mathbb{R}} a_m(x)a_n(x)p_c(x)\ \mathrm{d}x = \delta_{mn}. \quad (13)$$

In principle, p_0 and p_w can be any pdfs for which the integrals in (11) and (12) exist, and p_0 can be selected to entail known features of the exact solution [17], [19].

Definition 4 (Central-Gaussian distribution): In the following, $n_\sigma^{\text{central}}(x)$ denotes a central (i.e. zero-mean) Gaussian distribution with variance σ^2.

The following discussions are limited to central Gaussian $p_0(x)$ and $p_w(x)$ with variances σ_0^2 and σ_w^2.

III. SPARSITY OF THE SYSTEM MATRIX

As a result of the FPE being linear in $p(t,x)$, our approach is characterized by the matrix $\boldsymbol{H}$ in (5) and (8). In the stationary case, we need to algebraically solve the linear homogeneous system (8), whereas the transient case implies integration of the dynamic system (5). In both cases, it is critical that, as the size of $\boldsymbol{H}$ increases, only a small number of its elements are non-zero. In this section we discuss $\boldsymbol{H}$'s sparsity, which is a consequence of the orthogonality of the selected polynomial basis (13).

Although our approach is shown in Section V to outperform [18] both in the stationary and in the transient case, Section III-A revisits the structure of $\boldsymbol{H}$ for plain-polynomial test functions in view of the matrix properties discussed in Section II-C. Subsequently, Section III-B outlines how this structure changes for weighted-polynomial test functions.

A. Plain-polynomial test functions

In [18], plain basis polynomials are used as test functions, so that $\boldsymbol{v}(x) = \boldsymbol{a}(x)$ and $p_c(x) = p_0(x)$ in (13), and the resulting polynomial basis is a scaled generalization of Hermite-polynomials. The test function derivatives in (11) are given simply by the polynomial derivatives, $\boldsymbol{v}'(x) = \boldsymbol{a}'(x)$. Because the derivative of any polynomial can be expressed in terms of (lower-order) basis polynomials, $a'_m(x) = \sum_{k=0}^{m-1} \eta'_{mk} a_k(x)$, we can write

$$\boldsymbol{v}'(x) = \boldsymbol{E}'\boldsymbol{v}(x), \tag{14}$$

where $\boldsymbol{E}' = [\eta'_{n_1 n_2}] \in \mathbb{R}^{(N+1)\times(N+1)}$ is a lower-triangular matrix with zero-diagonal. Furthermore, Hermite polynomials have the convenient property that $a'_m(x) = \eta'_m a_{m-1}(x)$, which also applies for the scaled Hermite polynomials. As a result, $\boldsymbol{E}'$ has non-zeros only on the first sub-diagonal.

Due to Assumption 1, the drift term can be expressed in terms of the basis polynomials, $f(x) = \sum_{k=0}^{N} \eta_k^f a_k(x)$, given that $N^f \leq N$. Let $\mathbf{M} \in \mathbb{R}^{(N+1)\times(N+1)\times(N+1)}$ denote a symmetric three-way tensor whose elements are the weighted integrals over three basis polynomials,

$$m_{n_1 n_2 n_3} = \int_{\mathbb{R}} a_{n_1}(x) a_{n_2}(x) a_{n_3}(x) p_c(x) \mathrm{d}x. \tag{15}$$

We can now write

$$\boldsymbol{H}^f = \boldsymbol{E}' \sum_{k=0}^{N} \eta_k^f \boldsymbol{M}_k, \tag{16}$$

where $\boldsymbol{M}_k \in \mathbb{R}^{(N+1)\times(N+1)}$ is the kth matrix-slice of $\mathbf{M}$.

Remark 1: $\boldsymbol{M}_k$ is sparse for $k \ll N$, because $m_{n_1 n_2 n_3} = 0$ whenever $n_i > n_j + n_k$ for any i, j, k, due to the orthogonality of the basis polynomials.

Similar to (16), $\boldsymbol{H}^b$ is written as

$$\boldsymbol{H}^b = \underbrace{\boldsymbol{E}'\boldsymbol{E}'}_{\boldsymbol{E}''} \sum_{k=0}^{N} \eta_k^b \boldsymbol{M}_k. \tag{17}$$

In (17), $\boldsymbol{E}'' = \boldsymbol{E}'\boldsymbol{E}' \in \mathbb{R}^{(N+1)\times(N+1)}$ results from the second-order derivative representation of $\boldsymbol{v}(x)$ and has non-zeros only on the second sub-diagonal.

For illustration of the resulting $\boldsymbol{H}$-matrix we consider a 1D-DP (1) with cubical drift and additive diffusion,

$$f(x) = \beta x + \gamma x^3, \quad b(x) = \sigma^2, \tag{18}$$

where γ must be negative for stability. Fig. 1 (left) shows the sparsity pattern of $\boldsymbol{H}$ for (18) with $\beta, \gamma, \sigma \neq 0$.

Remark 2: The first row of $\boldsymbol{H}$ is always zero, which is a result of $\boldsymbol{E}'$'s and $\boldsymbol{E}''$'s first rows being zero. This guarantees at least one non-trivial stationary solution of (8), in accordance with Section II-C.

B. Weighted-polynomial test functions

This section inspects the structure of $\boldsymbol{H}$ for test functions with $p_w(x) = n^{\text{central}}_{\sigma_w}(x)$, so that the combined pdf is $p_c(x) = n^{\text{central}}_{\sigma_c}(x)$ with $\frac{1}{\sigma_c^2} = \frac{1}{\sigma_0^2} + \frac{1}{\sigma_w^2}$.

The derivatives of $\boldsymbol{v}(x)$ now involve derivation of the exponential function in $n^{\text{central}}_{\sigma_w}(x)$, so that $\boldsymbol{v}'(x)$ and $\boldsymbol{v}''(x)$ are no longer expressed by lower-order basis functions as in (14). Instead, application of the chain-rule results in

$$\boldsymbol{v}'(x) = \boldsymbol{E}'\boldsymbol{v}^{N+1}(x), \quad \boldsymbol{v}''(x) = \boldsymbol{E}''\boldsymbol{v}^{N+2}(x), \tag{19}$$

where $\boldsymbol{v}^{N+1}(x)$ and $\boldsymbol{v}^{N+2}(x)$ are obtained by expanding the test function basis with $v_{N+1}(x)$ and $v_{N+2}(x)$, and $\boldsymbol{E}' \in \mathbb{R}^{(N+1)\times(N+2)}$, $\boldsymbol{E}'' \in \mathbb{R}^{(N+1)\times(N+3)}$. Note that, although $v_{N+1}(x)$ and $v_{N+2}(x)$ are used to construct $\boldsymbol{H}$, they are not used as test functions in the Galerkin-scheme.

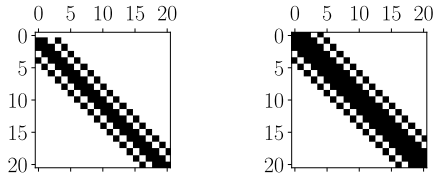

Fig. 1. Sparsity pattern of $\boldsymbol{H}$ for cubical diffusion process with additive noise (18), Gaussian $p_0(x)$ and $N = 20$. Left: Plain-polynomial test functions, Right: Gaussian $p_w(x)$.

$\boldsymbol{E}'$ and $\boldsymbol{E}''$ are no longer square and have non-zero elements below and above the diagonal. The sparsity of $\boldsymbol{H}$ for (18) and Gaussian $p_w(x)$ is shown in Fig. 1 (right).

Remark 3: For $\sigma_w < \infty$, the first row of $\boldsymbol{H}$ is no longer zero, so that the required zero-eigenvalue according to Section II-C is no longer obvious. Indeed, $\boldsymbol{H}$ may have full-rank for poorly chosen σ_w, but we observed in practice that σ_w can be selected to achieve the expected eigenvalue properties according to Section II-C.

Remark 4: For large σ_w, the weighting function $p_w(x)$ acts like a constant in the region of interest, and the test functions are equivalent to the plain polynomials. As a result, for $\sigma_w \to \infty$ the matrix $\boldsymbol{H}$ approaches the result from Section III-A, including the property that the first row is zero.

IV. MULTIVARIATE DIFFUSION PROCESSES

A. Multivariate diffusion process and FPE

Definition 5 (Multivariate diffusion process): In the multivariate case, we have $\boldsymbol{x}, \mathbf{X}_t \in \mathbb{R}^d$, and

$$\mathrm{d}\mathbf{X}_t = \boldsymbol{f}(\mathbf{X}_t)\mathrm{d}t + \boldsymbol{G}(\mathbf{X}_t)\mathrm{d}\mathbf{W}_t \tag{20}$$

describes a multivariate diffusion process, where $\mathbf{W}_t \in \mathbb{R}^{d_w}$ denotes the increment of a d_w-dimensional Wiener process.

Definition 6 (Multivariate Fokker-Planck equation): The corresponding FPE reads

$$\frac{\partial p(t,\boldsymbol{x})}{\partial t} = -\sum_{i=1}^{d} \frac{\partial}{\partial x_i} \left\{ p(t,\boldsymbol{x}) f_i(\boldsymbol{x}) \right\} + \frac{1}{2} \sum_{i=1}^{d} \sum_{j=1}^{d} \frac{\partial^2}{\partial x_i \partial x_j} \left\{ p(t,\boldsymbol{x}) B_{ij}(\boldsymbol{x}) \right\}, \tag{21}$$

where $\boldsymbol{B}(\boldsymbol{x}) = \boldsymbol{G}(\boldsymbol{x})\boldsymbol{G}(\boldsymbol{x})^T \in \mathbb{R}^{d\times d}$.

We search for approximate solutions of (21) of the form

$$\tilde{p}(t,\boldsymbol{x}) = \boldsymbol{u}(\boldsymbol{x})^T \boldsymbol{c}(t), \tag{22}$$

similar to (3), where univariate pdfs and polynomials are replaced by their multivariate counterparts, e.g.

$$u_{n_1,\cdots,n_d}(\boldsymbol{x}) = a_{n_1,\cdots,n_d}(\boldsymbol{x})p_0(\boldsymbol{x}). \tag{23}$$

If the maximum polynomial order for each state variable x_l is N_l, the dimension of U and V is $N_{\text{total}} = \prod_l (N_l + 1)$. The resulting matrix $\boldsymbol{H} \in \mathbb{R}^{N_{\text{total}} \times N_{\text{total}}}$ is given by

$$\boldsymbol{H} = \sum_{i=1}^{d} \boldsymbol{H}^{f_i} + \frac{1}{2}\sum_{i=1}^{d}\sum_{j=1}^{d} \boldsymbol{H}^{B_{ij}}, \tag{24}$$

where

$$\boldsymbol{H}^{f_i} = \int_{\mathbb{R}^d} \frac{\partial \boldsymbol{v}(\boldsymbol{x})}{\partial x_i} f_i(\boldsymbol{x}) \boldsymbol{u}(\boldsymbol{x})^T \mathrm{d}x_1 \cdots \mathrm{d}x_d \tag{25}$$

$$\boldsymbol{H}^{B_{ij}} = \int_{\mathbb{R}^d} \frac{\partial^2 \boldsymbol{v}(\boldsymbol{x})}{\partial x_i \partial x_j} B_{ij}(\boldsymbol{x}) \boldsymbol{u}(\boldsymbol{x})^T \mathrm{d}x_1 \cdots \mathrm{d}x_d, \tag{26}$$

after integration by parts, subject to equivalent assumptions about $p_0(\boldsymbol{x})$ and $p_w(\boldsymbol{x})$ as in Assumption 2.

B. Decoupled p_0, p_w, p_c

The computation of the integrals in $\boldsymbol{H}^{f_i}$ and $\boldsymbol{H}^{B_{ij}}$ is generally not tractable for higher system dimensions, such as $d > 3$. However, if we select $p_0(\boldsymbol{x})$ and $p_w(\boldsymbol{x})$ decoupled in the state variables, $p_0(\boldsymbol{x}) = p_0^{(1)}(x_1) \cdots p_0^{(d)}(x_d)$, then $\boldsymbol{u}(\boldsymbol{x})$ and $\boldsymbol{v}(\boldsymbol{x})$ can also be written in decoupled form, using univariate polynomials $\boldsymbol{a}^{(l)}(x_l)$ as in the 1D-case.

The partial derivatives in (25) are simply

$$\frac{\partial \boldsymbol{v}(\boldsymbol{x})}{\partial x_i} = v_{n_1}^{(1)}(x_1) \cdots v_{n_i}^{(i)\prime}(x_i) \cdots v_{n_d}^{(d)}(x_d), \tag{27}$$

and similarly for the second-order derivatives, meaning that all the derivative representations used in the 1D-case can be applied to the multivariate expressions in (25) and (26). Finally, the multivariate integrals can be computed as products of tractable univariate integrals in the state variables.

Note that it is possible to address strong dependence between some state variables by using partially coupled basis-functions, resulting in multivariate (but still low-dimensional) pdfs and polynomials, and their integrals. In this paper, however, we focus on fully decoupled basis-functions and their capabilities to reproduce even strongly coupled pdfs (see results in Sec. V).

For illustration we consider a 2D-diffusion process that describes a single-degree-of-freedom (SDOF) oscillator of Duffing type with external force excitation (additive noise) [17]. Let x_1 and x_2 denote the displacement and the velocity of a mechanical oscillator, and

$$\boldsymbol{f}(\boldsymbol{x}) = \left[x_2, f(x_1) + \varepsilon x_2\right]^T, \boldsymbol{B}(\boldsymbol{x}) = \mathrm{diag}(0, \sigma^2), \tag{28}$$

with $f(x)$ as in (18), and $\varepsilon < 0$ for the resulting system to be stable. The resulting sparsity pattern of $\boldsymbol{H}$ is shown in Fig. 2 (left) for Gaussian $p_0^{(1)}, p_w^{(1)}, p_0^{(2)}, p_w^{(2)}$.

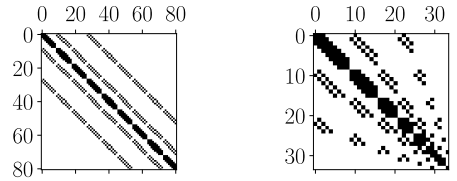

Fig. 2. Sparsity pattern of $\boldsymbol{H}$-matrix for Duffing-type diffusion process with additive noise (28) ($N_1 = N_2 = 8$) using Gaussian p_0, p_w. The HIT parameters are $q = \infty$ (no HIT active, left) and $q = 0.8$ (right). The order of the resulting systems is $N_{\text{total}} = 81$ and $N_{\text{total}} = 34$, respectively.

C. Hyperbolic index truncation

If the multivariate polynomials are expanded with equal order in each state, $N_1 = \cdots = N_d$, the overall system dimension N_{total} increases exponentially with d. In previous work [18], many of the N_l were hence kept at low orders, at the cost of depending on good initial approximations p_0.

In the context of polynomial chaos expansion it has been observed that expansion orders can be reduced for coupling terms between the states using *hyperbolic index truncation* (HIT) schemes [21]. In a similar spirit we define the set of admissible indices by

$$\mathcal{A}_q^{\boldsymbol{N}} \equiv \left\{ \boldsymbol{n} \in \mathbb{N}^d : \left(\sum_{l=1}^{d} \left(n_l / N_l\right)^q \right)^{\frac{1}{q}} \leq 1 \right\}, \tag{29}$$

with $q > 0$. For $q = \infty$, no HIT is active and *all* coupling polynomial terms are considered, equivalent to [18] and the system shown in Fig. 2 (left). Application of (29) with smaller q allows to maintain considerably higher expansion orders in each state dimension while managing the overall computational cost. Fig. 2 (right) shows the $\boldsymbol{H}$-matrix for an identical system and configuration where $q = 0.8$ in (29).

V. RESULTS

A. 1D-diffusion process

We begin by considering stationary solutions of the nonlinear system (18). For $\gamma < 0$, the exact solution reads

$$p_{\text{stat}}^{\text{exact}}(x) = c \exp\left(2\sigma^{-2} F(x)\right), \tag{30}$$

where $F'(x) = f(x)$ from (18) and c is a normalization constant, which can be verified by equating coefficients in the stationary FPE (2) with $\dot{p} = 0$.

We consider the following configurations for central Gaussian p_0 and p_w:

- "g-p": σ_0=1, σ_w=∞ (plain-*polynomial* v_n as in [18]).
- "g-w": σ_0=1, σ_w=1.2 (*weighted*-polynomial v_n).

Fig. 3 (left) shows the stationary pdf results and the error $err(x) = \tilde{p}_{\text{stat}}(x) - p_{\text{stat}}^{\text{exact}}(x)$ for $\beta = 1, \gamma = -0.2$ in (18) and $N = 30$, and demonstrates how weighted test functions outperform plain-polynomial test functions for identical p_0. Fig. 3 (right) shows the pdf-evolution over time initialized with a central-Gaussian pdf ($\sigma_{\text{init}} = 0.5$), compared with MCS using Euler-Maruyama integration and $N_{\text{MC}} = 10^5$ realizations.

The eigenvalues of the resulting $\boldsymbol{H}$-matrices for both configurations are as expected, according to Section II-C:

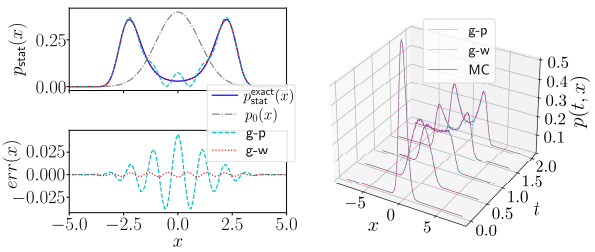

Fig. 3. Left: Stationary pdf and pdf error for Gaussian p_0, p_w with plain-polynomial ("g-p") and weighted-polynomial ("g-w") test functions for 1D-diffusion process (18), $N = 30$. The exact stationary solution and initial approximation $p_0(x)$ are also shown for reference. Right: Pdf-evolution $p(t,x)$ for (18), $N = 30$, compared with MCS ("MC") using Euler-Maruyama integration and $N_{\text{MC}} = 10^5$ realizations.

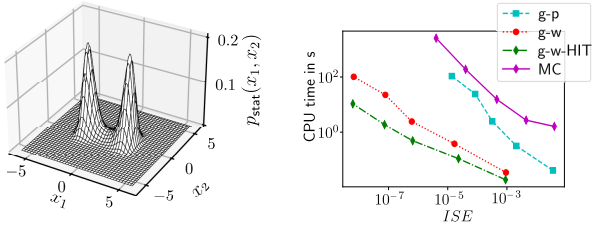

Fig. 4. Left: Stationary pdf $p_{\text{stat}}(x_1,x_2)$ for SDOF-oscillator (28) using "g-w-HIT" and $N_1 = N_2 = 30$. Right: Computation times required to achieve a certain accuracy for the stationary solution $p_{\text{stat}}(x_1,x_2)$ for (28). The polynomial expansion orders N_1, N_2 for "g-p", "g-w" and "g-w-HIT" were varied from 10 to 60. MCS result "MC" shown for comparison, with number of MC-realizations N_{MC} varied from 10^2 to 10^6.

All eigenvalues are negative except a single one that is zero, and the corresponding eigenvector represents the stationary solution of (8).

B. 2D-diffusion processes

For the 2D-diffusion process (28) we consider the same configurations as in the 1D-case, with identical σ_0^2 and σ_w^2 for x_1 and x_2. Further, a third configuration "g-w-HIT" is added with HIT-parameter $q = 0.8$. Fig. 4 (left) shows the stationary pdf for (28) using the "g-w-HIT"-configuration with expansion orders $N_i = 30$. The system size is $N_{\text{total}} = (30+1)^2 = 961$ for "g-p" and "g-w", and $N_{\text{total}} = 381$ for "g-w-HIT".

For negative γ in (18) and ε in (28), the exact stationary pdf for (28) reads

$$p_{\text{stat}}^{\text{exact}}(x_1,x_2) = c\exp\left(2\sigma^{-2}F(x_1)\right) n_{\sigma_2}^{\text{central}}(x_2), \qquad (31)$$

with $F'(x) = f(x)$ as in (30) and $\sigma_2^2 = -\frac{\sigma^2}{2\varepsilon}$ [17]. The fact that the 2D-example (28) has an exact stationary reference solution allows us to inspect how a desired accuracy affects the required computation times. Fig. 4 (right) shows the CPU times of "g-p", "g-w", "g-w-HIT" for varying polynomial expansion orders from $N_1, N_2 = 10$ to 60 over the integrated squared error $ISE = \int err(\boldsymbol{x})^2 \mathrm{d}\boldsymbol{x}$. For qualitative comparison, we also plot MCS computation times for varying numbers of realizations resulting in different accuracies. Stationary solutions are obtained by simulating over long enough periods of time T_{stat}, such that a quasi-stationary state is reached. $T_{\text{stat}} = 20$ was determined empirically, and the number of realizations was varied from $N_{\text{MC}} = 10^2$ to 10^6. All computations were performed using Python on a Dell computer with 12th Gen Intel(R) Core(TM) i7-1265U processor @ 1.8 GHz and 16GB RAM.

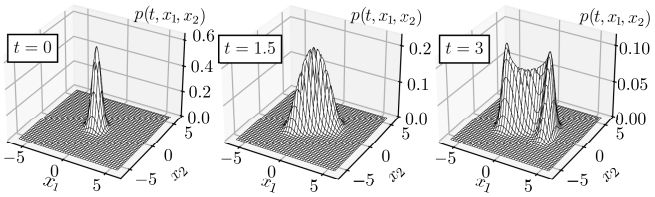

Fig. 5. Pdf-evolution $p(t,x_1,x_2)$ for SDOF-oscillator (28) using "g-w-HIT" and $N_1 = N_2 = 30$.

Remark 5: The comparison with MCS is only qualitative, as further optimization options such as parallelization or higher-order integration schemes were not explored.

Fig. 5 shows the pdf result for different t using "g-w-HIT" with $N_1 = N_2 = 30$, using a central Gaussian with covariance matrix $\boldsymbol{\Sigma}_{\text{init}} = \text{diag}\,(0.25, 0.25)$ as initial pdf.

C. 4D-diffusion process

We consider a system of 2 randomly excited Van-der-Pol oscillators, coupled via linear spring and damping elements,

$$\boldsymbol{f}(\boldsymbol{x}) = \begin{pmatrix} x_2 \\ \beta x_1 + \rho(1+\varepsilon x_1^2)x_2 + \gamma x_3 + \kappa x_4 \\ x_4 \\ \beta x_3 + \rho(1+\varepsilon x_3^2)x_4 + \gamma x_1 + \kappa x_2 \end{pmatrix}$$
$$\boldsymbol{B}(\boldsymbol{x}) = \text{diag}\left(0, \sigma^2, 0, \sigma^2\right), \qquad (32)$$

with parameter values $\rho = \gamma = \kappa = 0.2, \beta = -0.8, \varepsilon = -0.2, \sigma = 1$. A "g-w-HIT" configuration was used ($q = 1, N_i = 36$), resulting in $N_{\text{total}} = 91{,}376$ instead of $N_{\text{total}} = (36+1)^4 = 1{,}874{,}161$, and a matrix density of 7.9×10^{-7}.

For lack of exact stationary reference solutions, we use MCS to simulate over a long enough period of time to reach quasi-stationarity ($T_{\text{stat}} = 50$). Fig. 6 shows different stationary marginal pdfs as computed by the Galerkin-method (top) compared with MCS ($N_{\text{MC}} = 10^5$, bottom). Equation (8) was solved using an iterative least-squares solver from Python's `scipy.sparse` library in ∼20s for this configuration.

The deterministic Van-der-Pol oscillator exhibits a limit-cycle behavior that results in crater-like pdfs under stochastic excitation [23], which is preserved in $p_{\text{stat}}(x_1,x_2)$ of the 2DOF-system. Strong correlation between the displacements and velocities of the two bodies, due to the coupling spring and damping elements, is successfully reproduced in $p_{\text{stat}}(x_1,x_3)$ and $p_{\text{stat}}(x_2,x_4)$, in spite of assuming p_0 and p_w independent in the state variables (see Sec. IV-B).

Fig. 7 shows the transient 1D-marginal displacement and velocity densities of one of the oscillators, $p(t,x_1)$ and $p(t,x_2)$, compared with MCS ($N_{\text{MC}} = 10^5$). Here, the initial pdf was a Gaussian with mean $\boldsymbol{\mu}_{\text{init}} = (3,0,-3,0)^T$ and covariance matrix $\boldsymbol{\Sigma}_{\text{init}} = \text{diag}\,(0.5, 0.5, 0.5, 0.5)$.

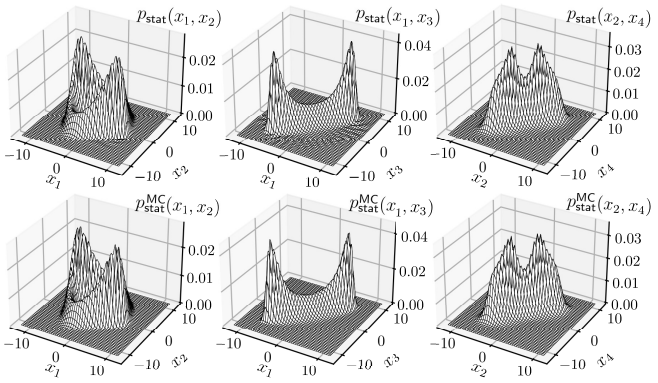

Fig. 6. Top row: Stationary marginal pdfs $p_{\text{stat}}(x_1, x_2)$, $p_{\text{stat}}(x_1, x_3)$, $p_{\text{stat}}(x_2, x_4)$ for 2DOF Van-der-Pol oscillator (32), $N_i = 36, q = 1$. Bottom row: MCS result at $T = 50$ for comparison using $N_{\text{MC}} = 10^5$ realizations.

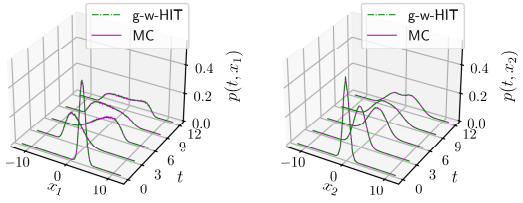

Fig. 7. Marginal pdf evolutions $p(t, x_1), p(t, x_2)$ for 2DOF Van-der-Pol oscillator (32), $N_i = 36, q = 1$. MCS result for comparison using $N_{\text{MC}} = 10^5$ realizations.

VI. SUMMARY AND DISCUSSION

We have demonstrated how the Galerkin-method presented in [17] and [18] can be generalized using weighted test functions. We discussed the structure of the resulting sparse linear systems, and applied hyperbolic index truncation to manage the computational cost for large systems. The performance was improved in the stationary case, and first results for transient FPE solutions were presented using this approach.

For the time being, suitable parameters for the initial approximation and weighting function are found empirically to yield non-positive eigenvalues according to Section II-C, but inappropriate parameters have been observed to lead to instability. A better understanding is necessary of what causes positive eigenvalues in the first place, so that suitable parameters can be found reliably for a given system. Furthermore, we expect that the structure and sparsity of the linear system for large expansion orders can be further exploited. Optimized solvers for high-dimensional systems could benefit from the specific structure, e.g. using sparse-tensor representations and tensor decompositions [24], [25].

The proposed method bears potential for nonlinear filtering due to its non-parametric and continuous representation of the pdf. We demonstrated how non-Gaussian pdfs can be propagated based on nonlinear system models, and the next step is to update the expansion coefficients based on nonlinear measurement models. A key question is how such updates can be realized directly, without the need to compute or integrate the underlying high-dimensional joint pdfs.

REFERENCES

[1] Ş. Aniţa, "Optimal Control of Stochastic Differential Equations via Fokker-Planck Equations," in Applied Mathematics and Optimization 84(2), 2021, pp. 1555–1583.

[2] M. Annunziato, A. Borzì, "Optimal control of probability density functions of stochastic processes," in Mathematical Modelling And Analysis 15(4), 2010, pp. 393–407.

[3] E. A. Buehler, J. A. Paulson, A. Mesbah, "Lyapunov-based stochastic nonlinear model predictive control: Shaping the state probability distribution functions," Proceedings of the American Control Conference (ACC), 2016, pp. 5389–5394.

[4] J. Zheng, G. Laparra, G. Zhu, M. Li, "Aggregate Power Control of Heterogeneous TCL Populations Governed by Fokker–Planck Equations," IEEE Transactions on Control Systems Technology, 28(5), pp. 1915–1927, 2020.

[5] A. Halder, R. Bhattacharya, "Probabilistic model validation for uncertain nonlinear systems," Automatica 50(8), 2014, pp. 2038–2050.

[6] F. Daum, "Nonlinear filters: beyond the Kalman filter," in IEEE Aerospace and Electronic Systems Magazine, 20(8), 2005, pp. 57–69.

[7] Y. Bar-Shalom, X.R. Li, T. Kirubarajan, "Estimation with Applications to Tracking and Navigation: Theory, Algorithms and Software," Wiley, 2004.

[8] S. Särkkä, "Bayesian Filtering and Smoothing," Cambridge University Press, 2013.

[9] C.W. Gardiner, "Handbook of Stochastic Methods," Third Edition, Springer, Berlin, 2004.

[10] F. Daum, J. Huang, "Particle degeneracy: root cause and solution," in Proceedings of SPIE - The International Society for Optical Engineering 8050, 2011.

[11] S. Challa and Y. Bar-Shalom, "Nonlinear filter design using Fokker-Planck-Kolmogorov probability density evolutions," IEEE Transactions on Aerospace and Electronic Systems, 36(1), pp. 309–315, 2000.

[12] M. Kumar, S. Chakravorty, "Nonlinear Filter Based on the Fokker-Planck Equation," Journal of Guidance, Control, and Dynamics, 35(1), p. 68–79, 2012.

[13] K.F. Caluya, A. Halder, "Proximal Recursion for Solving the Fokker-Planck Equation," Proceedings of the American Control Conference (ACC), 2019, pp. 4098-4103.

[14] C.S. Hsu, "Cell-to-Cell Mapping: A Method of Global Analysis for Nonlinear Systems," Springer, 2010.

[15] A. Naess and V. Moe, "Efficient path integration methods for nonlinear dynamic systems," in Probabilistic Engineering Mechanics, 15(2), 2000, pp. 221–231

[16] W.V. Wedig, U. von Wagner, "Extended Laguerre polynomials for nonlinear stochastic systems," in Computational Stochastic Mechanics, 1999, pp. 293–298.

[17] U. von Wagner, W.V. Wedig, "On the Calculation of Stationary Solutions of Multi-Dimensional Fokker-Planck Equations by Orthogonal Functions," in Nonlinear Dynamics 21, 2000, pp. 289–306.

[18] W. Martens, U. von Wagner, V. Mehrmann, "Calculation of high-dimensional probability density functions of stochastically excited nonlinear mechanical systems," in Nonlinear Dynamics 67(3), 2012, pp. 2089–2099.

[19] W. Martens, U. von Wagner, G. Litak, "Stationary response of nonlinear magneto-piezoelectric energy harvester systems under stochastic excitation," European Physical Journal Special Topics 222, 2013, pp. 1665–1673.

[20] D. Xiu, G.E. Karniadakis, "The Wiener–Askey Polynomial Chaos for Stochastic Differential Equations," in SIAM Journal on Scientific Computing 24(2), 2002, pp. 619–644.

[21] G. Blatman, B. Sudret, "Adaptive sparse polynomial chaos expansion based on least angle regression," in Journal of Computational Physics 230(6), 2011, pp. 2345–2367.

[22] F. Steppich, M. Gerdts, "Time Evolution of the State Probability Density Function by Iterative Polynomial Chaos Expansion," Proceedings of the European Control Conference (ECC), 2023.

[23] P. Kumar, S. Narayanan, "Solution of Fokker-Planck equation by finite element and finite difference methods for nonlinear systems," in Sadhana 31, 2006, pp. 445–461.

[24] Y. Sun, M. Kumar. "A tensor decomposition approach to high dimensional stationary Fokker-Planck equations," Proceedings of the American Control Conference (ACC), 2014.

[25] T.G. Kolda, B.W. Bader, "Tensor decompositions and applications," SIAM Review, 51(3), 2009, pp. 455–500.